that, at higher molecular energies, the density of higher energy states accessed in the hydrogen shift process prevails over the silyl shift process. We also note that reactions 13 and 14 predominate the dissociation over all energies; rates for this process are estimated to be 2-4 orders of magnitude faster than that for the 1,1 H_2 elimination (reaction 7) and 1,2 SiH_2 elimination (reaction 8). Taking the rate into account, the dominant pathway for decomposition is expected to be isomerization of ethynylsilane via reaction 9 followed by elimination of SiH_2 via reaction 16.

Conclusion

Primary dissociation pathways of ethynylsilane have been examined, and we find that pathways leading to the newly postulated species silylvinylidene, :CCH(SiH_3), are preferred energetically and kinetically. Silylvinylidene is suggested to be a transient species, which proceeds to dissociation, without barrier, to the products C_2H_2 and SiH_2. The net activation energy for the process is calculated to be 57.0 kcal/mol at the MP4SDTQ/6-31G* level of theory and is in good agreement with experiment. Other pathways leading to the observed products have been discounted. We note that C_2H_4 is a minor product of the decomposition studies of ethynylsilane.[1] No primary dissociation pathways of reasonable energy leading to C_2H_4 could be found. Consequently, we conclude that C_2H_4 results from secondary reactions.

Acknowledgment. We are grateful to Wayne State University Computer Center and Chemistry Department for provision of computing resources, the National Science Foundation for a Presidential Young Investigator Award (J.S.F.), and the NSF for Grant CHE-87-11901 (H.B.S.).

Tetrazetidine: Ab Initio Calculations and Experimental Approach

G. Ritter,[†,‡] G. Häfelinger,*[,†] E. Lüddecke,[§,⊥] and H. Rau*[,§]

Contribution from the Institut für Organische Chemie, Universität Tübingen, 7400 Tübingen, West Germany, and FG Physikalische Chemie, Institut für Chemie, Universität Hohenheim, 7000 Stuttgart 70, West Germany. *Received July 13, 1988*

Abstract: The kinetic analysis of the photoreaction system of azobenzenophanes is presented. We find, besides the cis and trans forms, a transient species living for a few minutes. All experimental evidence we have is compatible with a tetrazetidine structure of this species. The molecular structures of five configurational isomers of the hitherto unknown parent tetrazetidine have been calculated by ab initio restricted Hartree-Fock self-consistent field molecular orbital gradient optimizations using STO-3G, 6-31G, and 6-31G** basis sets. Geometries and total energies of the isomers with nonplanar, quadratic, and rectangular arrangements of the ring nitrogens are reported. The formation of tetrazetidine by approach to two *trans*-diazene molecules was simulated with optimization at all intermolecular separations R for a parallel [$\pi^2s + \pi^2s$] ground-state reaction pathway. Although all isomers of tetrazetidine are energetically less stable than their diazene dissociation products, the tetrazetidine seems to be trapped kinetically by rather high energy barriers.

1. Introduction

The four-membered ring system built only of nitrogen atoms is one of the few simple structures in organic chemistry that has not yet been synthesized. Indeed, a search for tetrazetidine in CAS-Online produces only the registry no. 58674-00-3 and two references which, however, do not mention the structure.

In the course of our investigations of the thermal and photoisomerization of the azobenzenophane **1**,[1] we realize some peculiarities that find an easy explanation if the formation of a tetrazetidine species **2** is assumed.

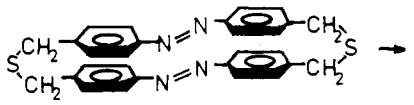

1

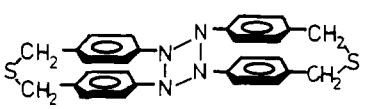

2

As the experimental evidence for the formation of a tetrazetidine structure is still indirect, we have tried to gain firm ground by employing ab initio restricted Hartree-Fock SCF MO calculations with analytical gradient optimization of possible molecular structure using STO-3G, 6-31G, and 6-31G** basis sets. Of course we had to restrict ourselves to the parent tetrazetidine system. These calculations are the first ones for tetrazetidine, and they give a result surprising for the organic chemist in that tetrazetidine should be a kinetically stable molecule accessible in a photoreaction.

2. Theoretical Approach to Tetrazetidine Formation

1. Ab Initio Calculations of the Molecular Structures and Stabilities for the Ground State of Configurational Isomers of Tetrazetidine. To the best of our knowledge no ab initio calculations of the molecular system of tetrazetidine are reported in the literature. There are, however, many calculations known for hydrazine[2-4] (**8**) and *trans*- and *cis*-diazene[4-9] (**9**, **10**) which are

† Universität Tübingen.
‡ Present address: Wella AG, Darmstadt, West Germany.
§ Universität Hohenheim.
⊥ Present address: BASF AG, Ludwigshafen, West Germany.

(1) Rau, H.; Lüddecke, E. *J. Am. Chem. Soc.* **1982**, *104*, 1616.
(2) Pasto, D. J. *J. Am. Chem. Soc.* **1979**, *101*, 6852-6857.
(3) Tanaka, N.; Hamada, Y.; Sugawara, Y.; Tsuboi, M. Kato, S., Morokuma, K. *J. Mol. Spectrosc.* **1983**, *99*, 245-262.
(4) Whiteside, A.; Binkley, J. S.; Krishnan, R.; DeFrees, D. J.; Schlegel, H. B.; Pople, A. J.: Carnegie-Mellon Quantum Chemistry Archive, Pittsburgh, 1980.
(5) Jensen, A. J. A.; Jorgensen, P.; Helgaker, T. *J. Am. Chem. Soc.* **1987**, *109*, 2895-2901.
(6) Winter, N. W.; Pitzer, R. M. *J. Chem. Phys.* **1975**, *62*, 1269-1275.
(7) Binkley, J. S.; Pople, J. A.; Hehre, W. J. *J. Am. Chem. Soc.* **1980**, *102*, 939-947.
(8) Pouchan, C.; Dargelos, A.; Chaillet, M. *J. Mol. Spectrosc.* **1979**, *76*, 118-130.

0002-7863/89/1511-4627$01.50/0

Table I. Results of ab Initio Optimizations of Molecular Structures of Seven Isomers of Tetrazetidine by Using STO-3G, 6-31G, and 3-31G** Basis Sets (Distances in angstroms, Angles in degrees, Energies in hartrees, and Dipole Moments in debyes)

		isomer of tetrazetidine						
parameter	basis	**3a**	**3b**	**4c**	**4b**	**5d**[f]	**6b**	**7b**
d_{NN}	STO-3G	1.4919	1.4920	1.5002 1.4901	1.4952	1.5001 1.4899	1.4996	1.4504
	6-31G	1.4692	1.4699	1.4840 1.4665	1.4747	1.4855 1.4640	1.4798	1.4336
	6-31G**	1.4384	1.4396	1.4528 1.4384	1.4453	1.4542 1.4358	1.4508	1.4149
d_{NH}	STO-3G	1.0489	1.0487	1.0489	1.0484	1.0493 1.0472 1.0504	1.0517	1.1043
	6-31G	0.9997	0.9997	1.0019	1.0016	1.0048 0.9980 1.0036	1.0067	0.9809
	6-31G**	1.0035	1.0034	1.0034	1.0030	1.0040 1.0014 1.0052	1.0060	0.9796
$\angle_{NNH}$	STO-3G	105.08	104.85	107.62 105.06	106.31	108.04 104.50 106.42 106.54	107.57	135.00
	6-31G	109.33	109.29	111.77 109.10	110.46	112.64 108.29 111.01 111.33	113.14	135.00
	6-31G**	106.86	106.97	109.46 106.84	108.13	110.09 106.18 108.50 108.75	110.26	135.00
E^{tot} [a]	STO-3G	−217.177 19	−217.177 00	−217.159 87	−217.159 02	−217.156 91	−217.131 55	−216.928 25
	6-31G	−219.806 95	−219.808 68	−219.784 04	−219.785 09	−219.782 54	−219.751 41	−219.640 28
	6-31G**	−219.950 14	−219.949 55	−219.931 24	−219.930 33	−219.929 09	−219.904 56	−219.742 66
E^{rep} [b]	STO-3G	129.373 69	129.462 95	129.098 80	129.115 27	129.105 25	128.663 48	130.204 49
	6-31G	131.625 29	131.522 47	130.993 30	131.039 85	130.993 70	130.343 47	132.223 24
	6-31G**	134.319 86	134.064 00	133.505 41	133.539 10	133.531 08	132.912 96	133.698 20
V/T [c]	STO-3G	2.011	2.011	2.011	2.011	2.011	2.011	2.011
	6-31G	1.999	1.999	1.999	1.999	1.999	1.999	1.999
	6-31G**	2.002	2.002	2.002	2.002	2.002	2.002	2.002
CONVG [d] × 10^{-12}	STO-3G	41.9	21.4	9.2	66.9	58.1	4.6	1.2
	6-31G	8.0	6.4	9.0	6.9	8.4	6.2	1.4
	6-31G**	5.8	25.9	6.5	5.9	76.2	7.0	5.1
$\vec{\mu}$ [e]	STO-3G	0.0	0.0	0.0	0.0	2.75	5.59	0.0
	6-31G	0.0	0.0	0.0	0.0	3.45	6.93	0.0
	6-31G**	0.0	0.0	0.0	0.0	2.90	5.85	0.0

[a] Total energies. [b] Nuclear repulsion energies. [c] Virial ratio of potential energy (V) and kinetic energy (T). [d] Reached criteria for convergence of optimization [hartrees]. [e] Calculated dipole moments. [f] Values for the deltoid structure given in the order distances: N2N3 = N3N4, N1N2 = N1N4; H1N1, H2N2 = H4N4, H3N3; angles: H3N3N2 = H3N3N4, H1N1N2 = H1N1N4, H2N2N3 = H4N4N3, H2N2N1 = H4N4N1.

of interest for comparison. In these calculations ab initio optimizations with various basis sets, (especially STO-3G, 3-21G, 4-31G, and 6-31G*) were carried out.

Our ab initio single-determinantal restricted Hartree–Fock SCF MO calculations[10-13] with full optimization of molecular structures using the analytical gradient technique of Murtagh and Sargent[14] have been performed with the GAUSSIAN-82 (G82) program system of Pople's group[15] in an IBM MVS version on a BASF 7/88 computer.[16] The following three standard Gaussian basis sets were used for this work: minimal, STO-3G;[17] split valence, 6-31G;[18] and split valence with polarization d functions on N and polarization p functions on H, 6-31 G**.[19]

The formulas of the isomers of tetrazetidine and related molecules studied are given in Figure 1. Four basic arrangements of the nitrogen nuclei have been considered: (a) nonplanar (butterfly), (b) planar quadratic, (c) planar rectangular, and (d) planar deltoid. All five possible hydrogen-substitution patterns (**3**–**7**) have been included. The nonplanar isomer **3a** with all hydrogen substituents in trans arrangement appeared as the most stable molecular form. If geometries were restricted to the quadratic arrangement (b), the corresponding isomer **3b** was the most stable one. If the rectangular geometry (c) was taken as a starting point, the structures converged to the quadratic isomers with exception of **4c** with two cis and trans configurations of the H atoms and the longer N–N bond between the cis hydrogens. An arrangement with the longer N–N bonds between the trans hydrogens also converges to the isomer **4c** during the optimization procedure. The isomer **5** with three hydrogens up and one down found its energetic minimum in a deltoid arrangement **5d**. The all cis isomer **6** and the totally planar isomer **7** (which is very unstable) prefer the quadratic forms **6b** and **7b**. No optimizations for geometries with nonplanar arrangement of nitrogens was performed for isomers **4**–**6**.

(9) Inagaki, S.; Goto, N. *J. Am. Chem. Soc.* **1987**, *109*, 3234–3240.
(10) Csizmadia, I. G. *Theory and Practice of MO Calculations on Organic Molecules*; Elsevier: Amsterdam, 1976.
(11) Carsky, P.; Urban, M. *Ab initio Calculations. Lecture Notes in Chemistry*; Springer: Berlin, 1980; Vol. 16.
(12) Szabo, S.; Ostlund, N. S. *Modern Quantum Chemistry. Introduction to Advanced Electron Structure Theory*; MacMillan: New York, 1982.
(13) Hehre, W. J.; Radom, L.; von Schleyer, P. R.; Pople, A. *Ab initio Molecular Orbital Theory*; Wiley: London, 1986.
(14) Murtagh, B. A.; Sargent, R. W. H. *Comput. J.* **1970**, *13*, 185–194.
(15) Binkley, J. S.; Frisch, M. J.; DeFrees, D. J.; Raghavachari, K.; Whiteside, A.; Schlegel, H. B.; Flunder, E. M.; Pople, J. A. *GAUSSIAN-82*; Carnegie-Mellon University, Pittsburgh, 1984.
(16) Calculations at the "Zentrum für Datenverarbeitung der Universität Tübingen". Installation of G82 by C. U. Regelmann.
(17) Hehre, W. J.; Stewart, R. F.; Pople, J. A. *J. Chem. Phys.* **1969**, *51*, 2657–2664.
(18) Hehre, W. J.; Ditchfield, R.; Pople, J. A. *J. Chem. Phys.* **1972**, *56*, 2257–2261.
(19) Hariharan, P. C.; Pople, J. A. *Theor. Chim. Acta* **1973**, *28*, 213–222.

Table II. Results of ab Initio Optimizations of Three Related Compounds for Comparison Using STO-3G,[7] 6-31G, and 6-31G** Basis Sets (Experimental Values: Hydrazine[20] (ED r_g), *trans*-Diazene[21] (IR r_z))

		compound		
		hydrazine	diazene	
parameter	basis	(**8**)	trans (**9**)	cis (**10**)
d_{NN}	STO-3G	1.4581	1.2668	1.2638
	6-31G	1.3964	1.2284	1.2274
	6-31G**	1.4111	1.2156	1.2147
	exptl	1.449 (2)	1.252 (2)	
d_{NH}	STO-3G	1.0394 1.0365	1.0611	1.0637
	6-31G	0.9952 0.9919	1.0117	1.0197
	6-31G**	1.0013 0.9983	1.0150	1.0182
	exptl	1.021 (2)	1.028 (5)	
$\angle_{NNH}$	STO-3G	109.01 105.43	105.27	111.49
	6-31G	116.97 113.34	110.56	116.02
	6-31G**	112.49 108.47	107.58	113.07
	exptl	112.0 (2) 106.0 (2)	106.8 (5)	
E^{tot} [a]	STO-3G	−109.748 06	−108.556 95	−108.545 24
	6-31G	−111.123 84	−109.929 46	−109.915 31
	6-31G**	−111.183 52	−110.001 23	−109.990 37
E^{rep} [b]	STO-3G			
	6-31G	42.239 89	32.641 11	32.520 94
	6-31G**	42.140 01	32.935 39	32.856 85
$-V/T$ [c]	STO-3G			
	6-31G	1.999	1.999	2.000
	6-31G**	2.002	2.002	2.002
CONVG[d] × 10^{-12}	STO-3G			
	6-31G	9.7	15.2	5.4
	6-31G**	24.8	1.2	7.0
$\vec{\mu}$ [e]	STO-3G	2.22	0.00	2.87
	6-31G	1.91	0.00	3.80
	6-31G**	2.16	0.00	3.20

[a–e] See footnotes for Table I.

The results of our calculations on tetrazetidines are collected in Table I. Values calculated with the same procedures and basis sets for the molecules **8–10** useful for comparison are shown in Table II. For all isomers in each basis set the calculated N–N distances are longer than those in hydrazine (**7**), whereas the N–H distances do not differ significantly.

Comparison of experimental geometeric parameters for hydrazine (**8**)[20] and *trans*-diazene (**9**)[21] with the calculated values of Table II show that STO-3G values agree much better with the experimental ones although total energies (which by use of the variation principle are indicators of the quality of the basis functions) are far lower for 6-31G and 6-31G** basis sets. Recently we have shown[22] that in the case of nonstrained hydrocarbons each standard Gaussian basis set may be used to predict various kinds of experimental distance parameters by regression equations with different statistical reliability. In that study[22] of eight basis sets it appears that the best one for prediction of geometries of hydrocarbons was 6-31G. We assume similar performance of basis sets for the nitrogen compounds studied here. But the presence of the lone-pair electrons on the N atoms leads to a much stronger deviation of geometries calculated at the single-determinantal Hartree–Fock limit from true experimental or theoretical r_e parameters. In other words, to derive highly accurate geometric parameters and energy values, we should apply configuration interaction (CI) calculations as reported by Tanaka et al.[3] for **8**, which, however, are beyond the aim of this first exploratory study of the hitherto unknown tetrazetidine system. In this study we rely on both 6-31G and 6-31G** values and infer that trends in the series of isomeric forms are predicted reliably.

Table III. Energetical Stabilities of Tetrazetidine Isomers Relative to Most Stable Isomer **3a** (kcal/mol)

	basis set		
isomer	STO-3G	6-31G	6-31G**
3a	0.0	0.0	0.0
3b	0.118	0.080	0.372
4c	10.866	13.119	11.860
4b	11.399	13.718	12.431
5d	12.722	15.317	13.207
6b	28.641	34.853	28.603
7b	156.212	104.588	130.199

The total energies of all seven stable tetrazetidine isomers relative to that of **3a** are given in Table III. The trends are rather similar for all three applied basis sets: 6-31G** gives the lowest values for total energies. There is only a small but significant difference of 0.4 kcal/mol of the stabilities of the nonplanar (**3a**) and planar (**3b**) conformers with alternating arrangement of the hydrogen atoms. The difference between the energies of optimized quadratic (**4b**) and rectangular (**4c**) forms of the isomer **4** is 0.6 kcal/mol. To our surprise the deltoid form **5d** turned out to be relatively stable. The totally planar molecule, which is isoelectronic to a cyclobutadiene tetraanion, is unstable by more than 100 kcal/mol.

In Figure 2 the 6-31G valence MOs of the most stable isomers **3–7** of tetrazetidine are given in comparison to those of trans and cis diazene. For the highly symmetric isomers with high symmetry **3a**, **3b**, **6b**, and **7b** these MOs refer to a kind of Walsh orbitals[23] in a cyclobutane-like situation[24] in which the nitrogen $2p_x$ and $2p_y$ atomic orbitals are directed parallel to the diagonals of the nitrogen quadrangle. The nitrogen $2p_z$ AOs contribute as well to NH bonding as to lone-pair character. In terms of symmetry-adapted MOs one observes for the tetrazetidine isomers with high symmetry a MO pattern that is very similar to the well-known one of the π-MOs of cyclobutadiene: This is seen clearly in the case of the four doubly occupied N(1s) core-electron MOs around 15.65 hartrees, which are not shown in Figure 2, and also in the case of the lowest valence MOs 5–8 between −1.5 and −0.9 hartrees, which indicate mostly N–N and N–H bonding between N(2s) and H(1s) AOs. All other MOs show strong mixing of all N and H AOs. For all isomers **3–7** the HOMO 16 shows leading lone-pair character due to N($2p_z$) contribution.

2. Ab Initio Calculations for Ground-State Cycloaddition for Two *trans*-Diazene Molecules. As may be seen from the values presented in Tables I and II even the most stable isomeric tetrazetidine **3a** is destabilized by 33 kcal/mol with respect to two isolated trans diazene molecules (**9**). But our calculations give stable tetrazetidine molecules with defined geometries for all isomers **3–7**. This may be an indication of a kinetically trapped molecule. Therefore we have calculated (in 6-31G and 6-31G**) the total energies of the supermolecular system "two *trans*-diimide molecules" approaching in two different manners: in an approach of two *trans*-diazene molecules **9** leading to the product **3b** and in a different parallel approach leading to **4c**. Both correspond to the Woodward–Hoffmann-forbidden [$\pi^2s + \pi^2s$] ground-state cyclization. In Table IV the total energies are presented as a function of the separation R with optimization of molecular geometries at each value of R. The numbers for both basis sets indicate an energy barrier of more than 120 kcal/mol for the thermal formation of **3b**.

In Figure 3 the ground-state energy profile for the cyclization reaction leading to **4c** is shown. The absolute value of the barrier

(20) Kohata, K.; Fukuyama, T.; Kichutsu, K. *J. Phys. Chem.* **1982**, *86*, 602–606.
(21) Carlotti, M.; Jones, J. W. C.; Trombetti, A. *Can. J. Phys.* **1974**, *52*, 340–344.
(22) Häfelinger, G.; Regelmann, C. U.; Krygowski, T. M.; Wozniak, K., submitted to *J. Comput. Chem.*
(23) Walsh, A. D. *Trans. Faraday Soc.* **1949**, *45*, 179.
(24) Klessinger, M. *Elektronenstruktur organischer Moleküle, Grundbegriffe quantenchemischer Betrachtungsweisen*; Verlag Chemie: Weinheim, 1982; p 104.

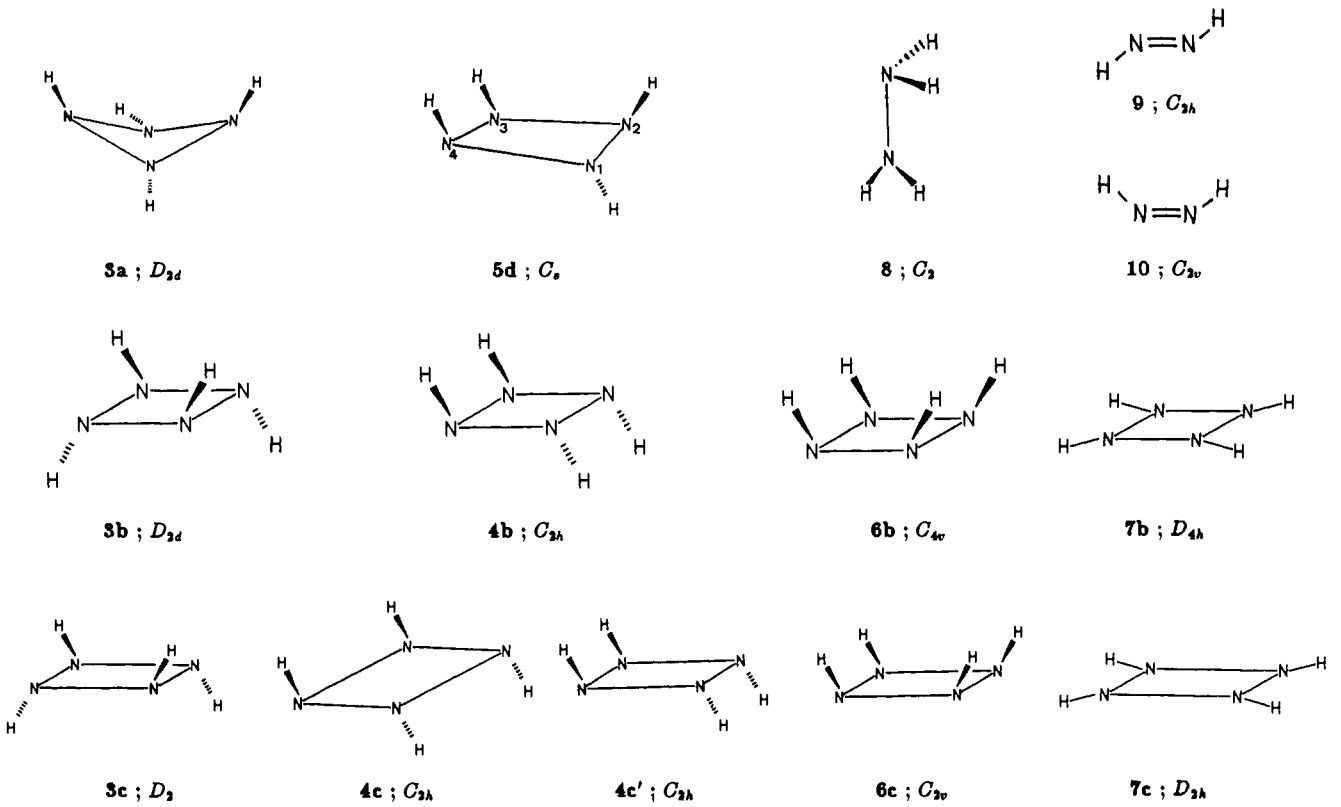

Figure 1. Numbering, molecular structures, and symmetry point groups for tetrazetidine isomers **3–7** and related molecules **8–10** (a, nonplanar nitrogens; b, nitrogens planar quadratic; c, nitrogens planar rectangular; d, nitrogens planar deltoid).

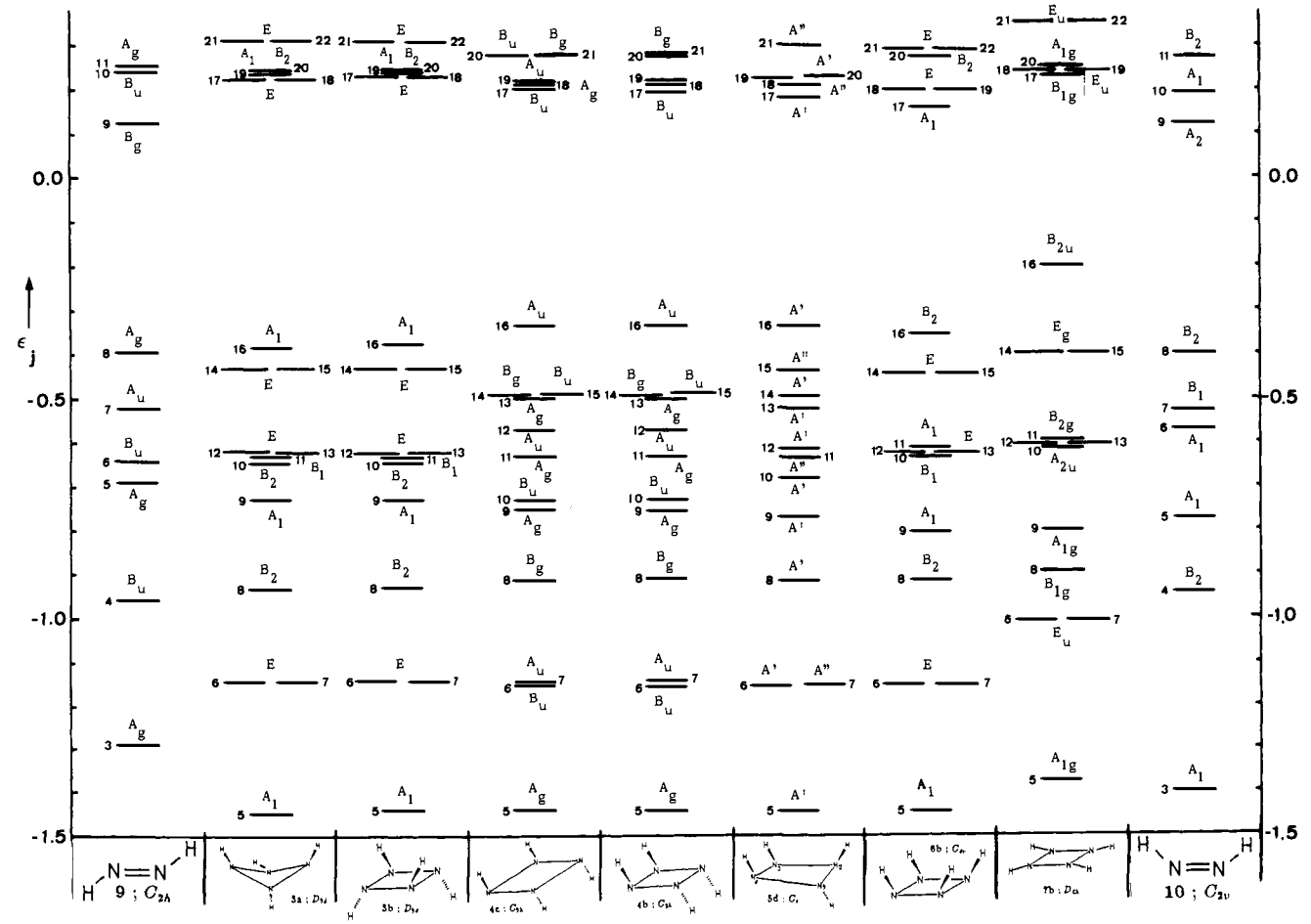

Figure 2. Calculated 6-31G valence MOs for tetrazetidines **3–7** and diazenes 9 and **10**.

heights seems to be too large. As mentioned before a CI treatment should be conducted for these reacting systems, which is, however, beyond our calculation capacities. We expect that an improvement by CI calculations would refine the numerical results but not,

Table IV. 6-31G and 6-31G** Calculated Total Energies (hartrees) for Two Parallel Molecules **9** Leading either to **3a** or to **4c** with Molecular Optimizations in Dependence on Distance of Molecular Separations *R*

	"product" 4c		"product" 3b	
R, Å	6-31G	6-31G**	6-31G	6-31G**
4.0	−219.858 09	−220.001 92	−219.859 74	−220.003 07
3.5	−219.856 93	−220.001 08	−219.859 90	−220.003 14
3.0	−219.851 17	−219.996 15	−219.856 82	−220.000 05
2.5	−219.824 79	−219.971 30	−219.836 27	−219.979 33
2.4	−219.812 68	−219.959 70	−219.826 02	−219.969 08
2.3	−219.796 20	−219.943 90	−219.811 74	−219.954 92
2.2	−219.773 77	−219.922 43	−219.791 94	−219.935 44
2.1	−219.743 30	−219.893 38	−219.764 65	−219.908 84
2.0	−219.702 02	−219.854 21	−219.727 22	−219.872 72
1.9	−219.646 24	−219.801 56	−219.676 19	−219.823 92
1.8	−219.719 54	−219.842 77	−219.734 57	−219.854 26
1.7	−219.750 23	−219.878 83	−219.766 55	−219.891 66
1.6	−219.773 99	−219.909 33	−219.791 86	−219.923 73
1.5	−219.785 77	−219.928 56	−219.805 88	−219.945 20
1.4	−219.777 01	−219.927 18	−219.800 67	−219.947 30
1.3	−219.732 68	−219.889 67	−219.762 18	−219.915 47
1.2	−219.626 50	−219.790 21	−219.665 78	−219.825 59
1.1	−219.413 61	−219.585 57	−219.470 07	−219.638 02
1.4699[a]			−219.806 82	
1.4396[a]				−219.949 55
1.4665[b]	−219.786 04			
1.4384[b]		−219.931 24		
2 × 9[c]	−219.858 91	−220.002 46	−219.858 91	−220.002 46
Δ[d]	45.73	44.69	32.69	33.20

[a] Values for the tetrazetidine isomer **3b**. [b] Values for the tetrazetidine isomer **4c**. [c] Reference energies for two *trans*-diazene molecules **9**. [d] Calculated destabilization of tetrazetidine isomers with respect to two molecules **9** in kcal/mol.

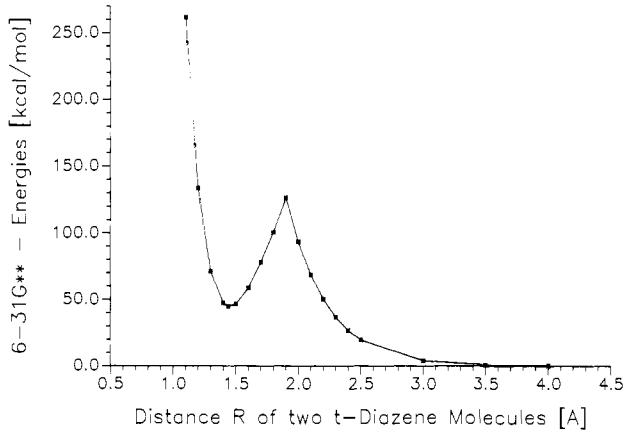

Figure 3. Total energy of the system "two *trans*-diazenes"/tetrazetidine vs distance *R* of the *trans*-diazene units (6-31G** results), parallel approach → **3b**: [π^2s + π^2s].

however, the fundamental statements.

3. Correlation Diagrams. The state correlation diagram of the [π^2s + π^2s] cycloaddition of two ethylene molecules to form cyclobutane is well-known.[25] In this section we scrutinize the influence of the n orbitals at the nitrogens, i.e., whether or not a cycloaddition reaction may be predicted for n → π^* and π → π^* excitations in the *trans*-diazene system.

Although the calculations in section 2.1 have shown that the tetrazetidine with the hydrogen atoms in an alternating sequence (**3a**) is the most stable isomer, we take the cis–trans structure (**4c**) as a starting point for the development of the correlation diagrams as according to the X-ray structure this configuration is preformed in the azobenzenophanes.[26] Then the reaction is to be classified according to C_{2h} symmetry with the C_2 axis being that of the individual azo groups. The orbital correlation diagram of Figure 4 has been constructed from the 6-31G data of Table IV. The correlations connecting the MOs were developed from the symmetries of the MOs and the leading AO contributions. Figure 5 shows a qualitative state correlation diagram including those states of the tetrazetidine that are correlated to the G, (n,π^*), (π,π^*), and (π,π^*)^2 states of the diazenes. Although no CI treatment was performed, we used the results of the calculations

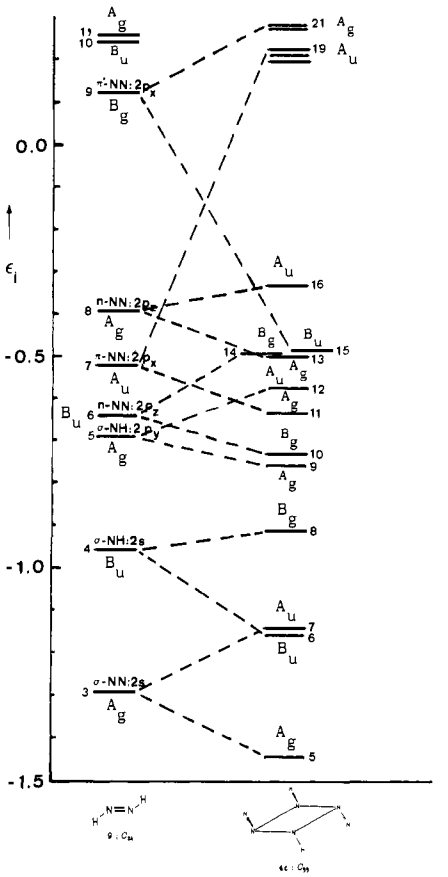

Figure 4. (6-31G) orbital correlation diagram for the **9** → **4c** [π^2s + π^2s] cycloaddition of two *trans*-diazene molecules.

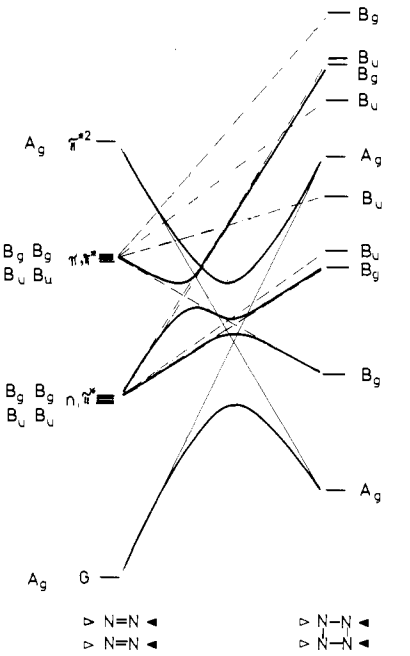

Figure 5. Qualitative state correlation diagram for the **9** → **4c** [π^2s + π^2s] cycloaddition of two *trans*-diazene molecules.

(25) Anh, N. T. *Die Woodward-Hoffmann-Regeln und ihre Anwendung*; Verlag Chemie: Weinheim, 1972; p 114.
(26) Sawitzki, G., Rau, H. *Liebigs Ann. Chem.* **1981**, 993–998.

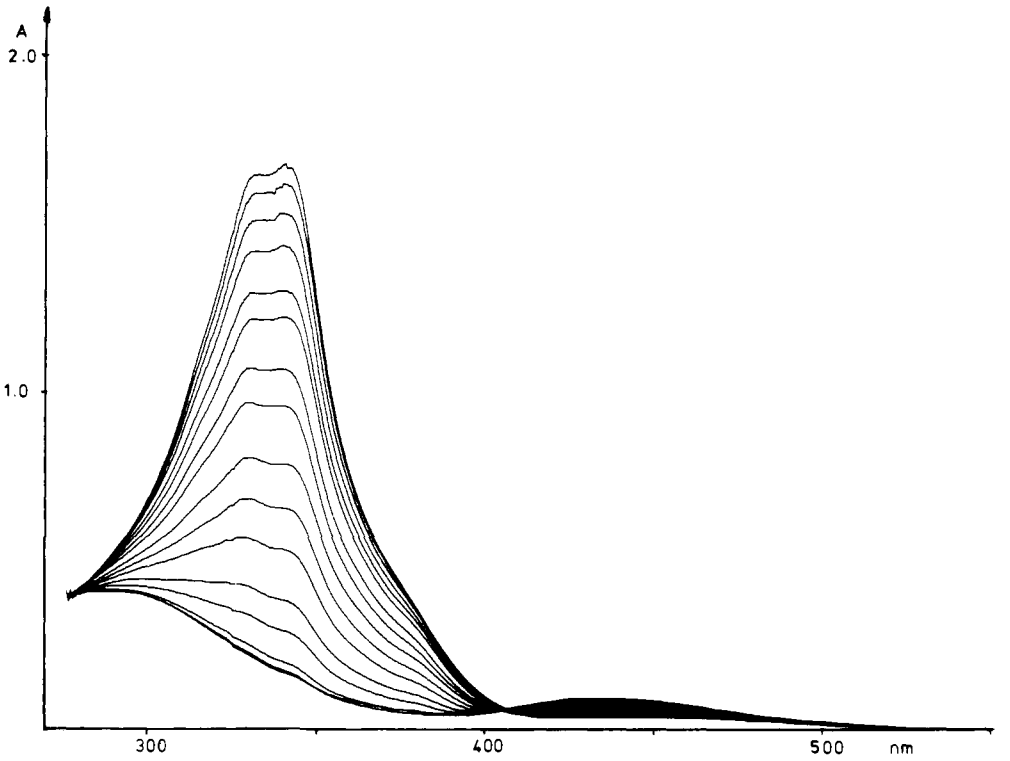

Figure 6. Photoreaction spectra of **1** on 366-nm irradiation.

as a guideline for placing the energies of the tetrazetidine states: The ground state is higher in energy than that of the two diazenes **9**, and the main contribution to energy change in the cycloaddition reaction is due to π to π^* interconversion leading to stabilization (π^* correlates to π) or destabilization (π correlates to π^*). Thus the states of tetrazetidine can be grouped according to the number of stabilizing and destabilizing correlations on tetrazetidine formation: (a) one $\pi^* \rightarrow \pi$ stabilizing and one $\pi \rightarrow \pi^*$ destabilizing correlation, B_g from $B_g(\pi,\pi^*)$; (b) one stabilizing $\pi^* \rightarrow \pi$ and two destabilizing $\pi \rightarrow \pi^*$ correlations, B_g from $B_g(n,\pi^*)$, B_u from $B_u(n,\pi^*)$, and B_u from $B_u(\pi,\pi^*)$; (c) two destabilizing $\pi \rightarrow \pi^*$ correlations, A_g from $A_g(G)$; (d) one destabilizing $\pi \rightarrow \pi^*$ and one destabilizing $\pi^* \rightarrow \pi^*$ correlation, B_u from $B_u(\pi,\pi^*)$; (e) two destabilizing $\pi \rightarrow \pi^*$ and one destablizing $\pi^* \rightarrow \pi^*$ correlation, B_g from $B_g(n,\pi^*)$, B_u from $B_u(n,\pi^*)$, and B_g from $B_g(\pi,\pi^*)$.

The state correlation diagrams show that the ground-state [π^2s + π^2s] cycloaddition reaction is symmetry forbidden. The correlation of diazene (n,π^*) states to tetrazetidine states is uphill; therefore, the photoreaction starting from this state is unfavorable. But there is a chance for the reaction in the (π,π^*) state. The diagram of Figure 5 would suggest the same type of reaction as in ethylene dimerization; the exact shape of the total energy surfaces would determine the yield of the reaction.

3. Experimental Approach to Tetrazetidine Formation: Photochemistry of Azobenzenophane

The azobenzenophane **1** shows a slightly modified azobenzene absorption spectrum (Figure 6) with the characteristic long-wavelength $n \rightarrow \pi^*$ band (λ_m = 436 nm, ϵ = 1400 dm^3 mol^{-1} cm^{-1}) and the first $\pi \rightarrow \pi^*$ band in the near UV (λ_{max} = 340 nm, ϵ_{340} = 50.500 dm^3 mol^{-1} cm^{-1}). The absorption coefficients are roughly 2 times as large as those of an azobenzene unit; a new band appearing as a shoulder at 380 nm is indicative of the phane structure. The phane shows a photoreaction (Figure 6) whose spectra can be analyzed by the Mauser diagnostics[27] (see Appendix), which can be used to find the number s of independent reactions in a reaction system. We have shown in 1982[1] that the photoinduced and thermal reactions of **1** are predominantly trans–cis isomerizations and have proved thus the existence of an inversion mechanism. However, we mentioned then another re-

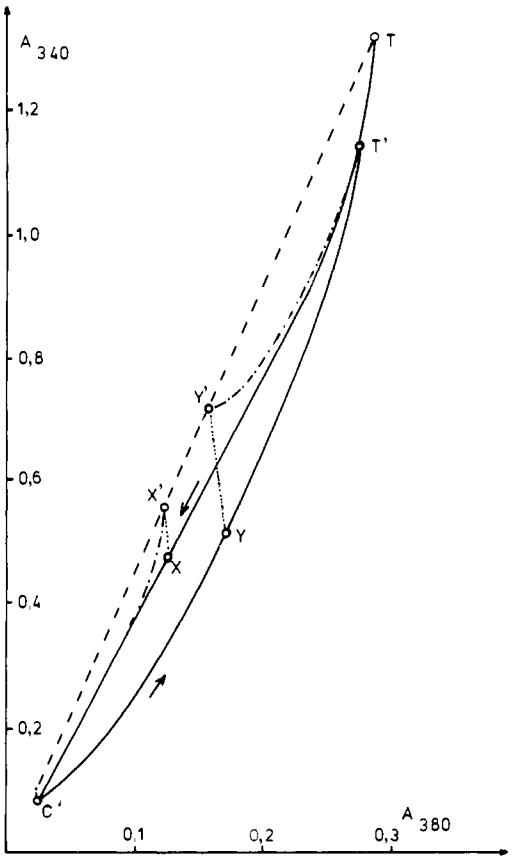

Figure 7. Mauser A diagram of the reaction system of **1**: T, pure tt; T′, photostationary state at 436-nm irradiation; C′, photostationary state at 366-nm irradiation. T′ → X → C′, 366-nm-induced reaction; C′ → Y → T′, 436-nm-induced reaction; Y → Y′ → T, fast and slow thermal back reaction to tt; Y → Y′ → T′, fast dark reaction and resumed 366-nm irradiation.

(27) (a) Mauser, H. *Formale Kinetik*; Bertelsmann Universitätsverlag: Düsseldorf, 1974. (b) Mauser, H. *Z. Naturforsch.* **1968**, *23b*, 1025–1033.
(28) Berning, W.; Hünig, S. *Angew. Chem., Int. Ed. Engl.* **1977**, *16*, 777.
(29) Kungler, O.; Prinzbach, H. *Angew. Chem., Int. Ed. Engl.* **1987**, *26*, 566.

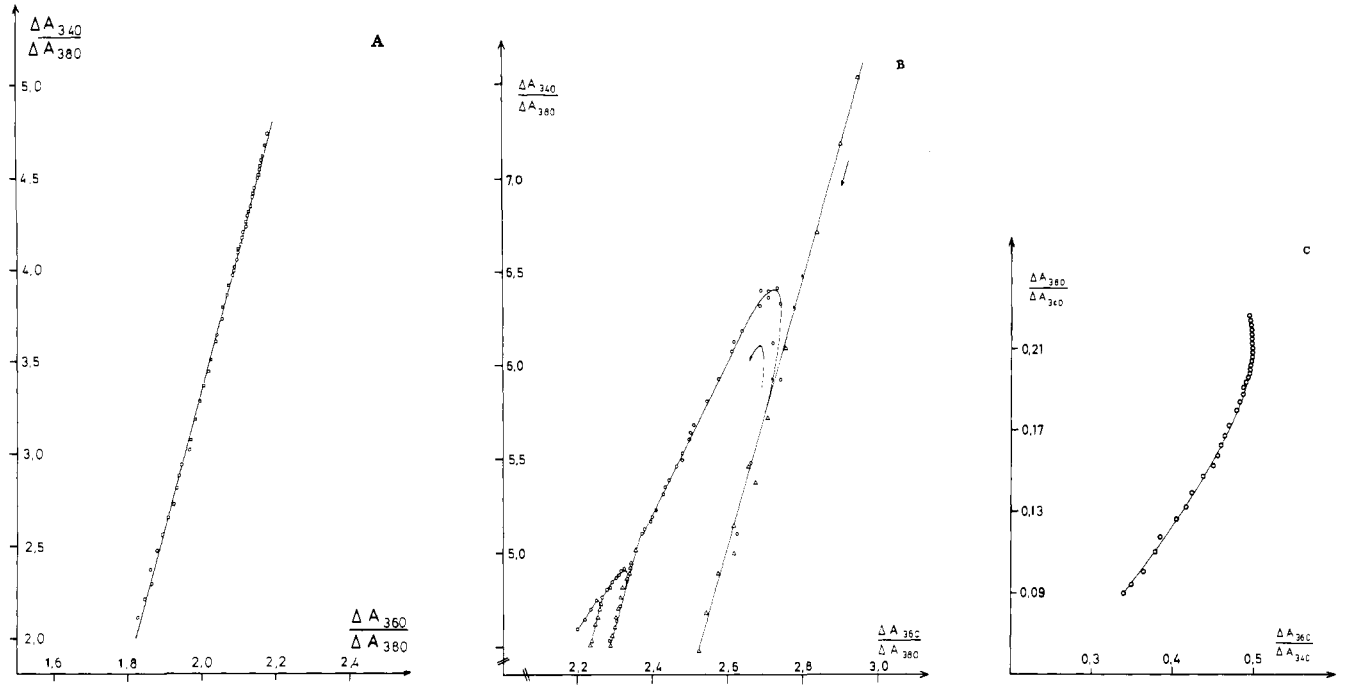

Figure 8. (A) Mauser ADQ2 diagram of the 436-nm photoreaction of **1** (○) with intermitted dark reaction phases (△). (B) Mauser ADQ2 diagram of the 366-nm photoreaction of **1** (○) with intermitted dark reaction phases (△). (C) Mauser ADQ2 diagram of the 366-nm photoreaction of **1** without dark reaction phases.

versible reaction on 366-nm irradiation on which we focus in this paper.

Figure 7 shows the absorbance (A_{λ_α} vs A_{λ_β}) diagram for 436- (i.e., n → π^* excitation) and 366-nm irradiation (i.e., $\pi \rightarrow \pi^*$ excitation) and the dark reactions. We selected λ_α at the azobenzene UV-band maximum and λ_β in the region of the cyclophane band (according to the recommendations given in the Appendix); other wavelength combinations give the same qualitative results. We have run numerous cycles of isomerizations with 366-nm irradiation to shift the system toward cis and with 436-nm irradiation to shift the system back to trans and have always reached the same points T′ and C′ in the *A* diagram within spectrophotometric accuracy. No material is lost in side reactions. Figure 8A is the Mauser ADQ diagram, a plot of the ratios of absorbances ($\Delta A_{\lambda_\alpha}/\Delta A_{\lambda_\beta}$ vs $\Delta A_{\lambda_\gamma}/\Delta A_{\lambda_\beta}$), for 436-nm irradiation and intermittent dark periods, Figure 8B is the same diagram for 366-nm irradiation, and Figure 8C is an ADQ plot for the photoreaction on 366-nm irradiation only. The wavelength λ_γ was chosen arbitrarily.

The *A* diagrams of the photoreactions in Figure 7 do not conform to eq 5 of the Appendix. The nonlinear plots indicate that there is more than one photoreaction active at both 436- and 366-nm irradiation. The *A* diagrams of the dark reactions in Figure 7 reveal two consecutive $s = 1$ reactions. The linear ADQ2 diagram of Figure 8A is in accord with eq 9 of the Appendix and shows that only two independent reactions occur on 436-nm irradiation. The thermal reactions are the same as the light-induced ones. However, there are more than two reactions at 366-nm irradiation as is indicated by the nonlinear plot in Figure 8B,C. It should be noted that for the lines in the diagrams of Figure 7 close to 100 data points for one isomerization reaction have been taken. The experimental details have been reported in ref 1.

The following reaction schemes are reasonable and in agreement with the kinetic analysis:

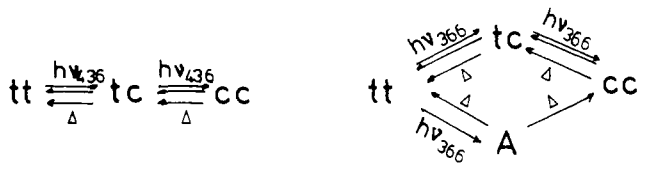

where tt stands for both azobenzene units in trans configuration. tc and cc are used correspondingly. A is an additional molecular form, whose nature will be discussed in the next section.

These reaction schemes are not sufficient for 313-nm irradiation, which irreversibly changes the spectrum of the azobenzenophane system. Photolysis at this wavelength leads to an unspecific absorption spectrum clearly indicating that the azobenzene units are destroyed.

4. Discussion: A Tetrazetidine?

The hidden reaction in 366-nm photochemistry (π,π^* excitation) which we considered "really unimportant" in 1982[1] may represent the first experimental observation of a tetrazetidine formation. We discuss the hypothesis that A be **2** on the basis of the results of the previous sections and some additional information.

1. The formation of a tetrazetidine A is in competition with isomerization in the excited state. The latter is very fast, so especially favorable conditions are a must if a tetrazetidine should be observed at all. A bimolecular cyclization reaction to form tetrazetidine would have no chance. This has been recognized by other groups also.[28,29]

2. Tetrazetidine is a kinetically stable molecule with defined geometry as follows from the calculations presented in section 2.1.

3. On excitation of the (n,π^*) state no species A is formed, but A is formed on $\pi \rightarrow \pi^*$ excitation. This is in accord with the qualitative considerations about tetrazetidine formation in section 2.3.

4. A formed in the azobenzenophane system is short lived, with a lifetime at most in the order of a few minutes, like the tc isomer of the phane from which it cannot be discriminated in terms of thermal stability. This is at variance from the expectations we have from the calculation of the ground-state stability of tetrazetidine in section 2.2. However, there may be some other nonparallel reaction path of tetrazetidine dissociation, in a sense a reversal of a Woodward–Hoffmann-allowed [π^2s + π^2a] cyclization with a lower barrier. Also we have not been able to include the influence of the phenyl rings in our calculations.

5. The thermal reaction leads back exclusively to the phane. The fragmentation reaction to form two isolated cis azobenzene units does not occur at all. This is rationalized by considering the high strain in these cis molecules.[30] Funke and Grützmacher

(30) One of us thanks Prof. Newkome, Baton Rouge, LA, for pointing this out.

have synthesized a series of p,p'-bridged *cis*-azobenzenes but have not been able to prepare the one with a $-CH_2-S-CH_2$ bridge.[31]

6. When the irradiation is carried out at 313 nm, the azobenzophane is totally destroyed. A tetrazetidine species **2** will have an absorption spectrum similar to that of hydrazobenzene, i.e., **2** should not absorb at 366 nm but should be excited at 313 nm. This excitation would disrupt the four membered ring, as it can be inferred for A in the photoreaction system of the phane. This unspecific degradation is tied to the phane structure: if the molecule with the open structure (**11**) or if a polymer $[-SCH_2C_6H_4N{=}NC_6H_4CH_2-]_n$ is irradiated under the same conditions, there is only trans–cis isomerization observed, independent of the wavelengths of excitation.

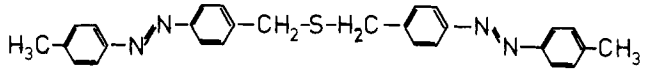

11

We have not found severe evidence against the possible formation of a tetrazetidine. The most serious objection comes from our calculations which predict that the tetrazetidine should be rather stable. However, as mentioned earlier, the calculations do not contain a CI treatment and thus overestimate the barrier height severely. An alternative valence isomerization leading to molecules like **12** or **13** can be excluded rather safely. Structure

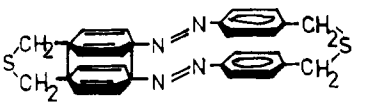

12

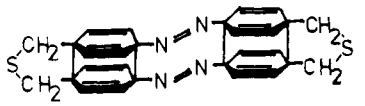

13

12 should still have an absorption at 366 nm, which would cause the aromatic/aliphatic azo compound to degrade, and structure **13** would require a tremendous rearrangement of bonds, leading to an extremely strained molecule.

The variations of experimental conditions usually employed in situations like the one we are in are not applicable here. The azobenzenophane **1** is only very slightly soluble. At room temperature the solubility in polarizable solvents like toluene is about 4×10^{-5} M at most. Low-temperature experiments soon find their limit in precipitation. We have tried to do low-temperature solid-state irradiations and have irradiated matrix-isolated molecules with UV detection.[32] However, the small changes in the absorption spectra were not helpful for the problem of this paper. The tetrazetidine as an isolated chemical still is elusive.

Acknowledgment. We are thankful for the support of the Deutsche Forschungsgemeinschaft, Bonn, and the Fonds der Chemischen Industrie, Frankfurt. Prof. Mauser and Prof. Gauglitz, Tübingen, have made available their sophisticated apparatus, which is gratefully acknowledged.

Appendix:[37] Reaction-System Analysis by Mauser Diagrams

H. Mauser has developed a method to analyze reaction systems of arbitrary complexity[27] by their kinetic behavior. Here a very short presentation pertinent to this paper is given; detailed information is to be found in the literature.

If there are s independent reactions taking place simultaneously (parallel and/or consecutive reactions), the change of absorbance (optical density) ΔA_λ at arbitrary wavelength λ is determined by the change of the concentrations of the i compounds in the reaction system:

$$\Delta A_\lambda(t) = \epsilon_{\lambda 1}\Delta c_1(t) + \epsilon_{\lambda 2}\Delta c_2(t) + \ldots = \sum_{j=1}^{i}\epsilon_{\lambda j}\Delta c_j(t) \quad (1)$$

Each compound's concentration is changed by each of the reactions k the compound takes part in. At any time the extent of reaction $\zeta_k(t)$[33] determines the amount of each compound j destroyed or created in this reaction k. So for one compound j taking part in k reactions with the respective stochiometric factors ν_{kj} the change in concentration is

$$\Delta c_j(t) = c_j(t) - c_{0j} = \sum_{k=1}^{s}\nu_{kj}\zeta_k(t) \quad (2)$$

and the OD change of the reaction mixture is

$$\Delta A_\lambda(t) = \sum_{j=1}^{i}\sum_{k=1}^{s}\epsilon_{\lambda j}\nu_{kj}\zeta_k(t) \quad (3)$$

The plots called Mauser diagrams are graphs of this master equation for $s = 1, 2, \ldots$ independent reactions if ΔA values at different wavelengths but at identical times are used to eliminate the $\zeta_k(t)$.

The Case $s = 1$. An example is $X \rightarrow B + C$. Then according to (3)

$$\Delta A_\lambda = \sum_{j=X}^{C}\sum_{k=1}^{1}\epsilon_{\lambda j}\nu_{kj}\zeta_k(t) = (\epsilon_{\lambda X}(-1) + \epsilon_{\lambda B}1 + \epsilon_{\lambda C}1)\zeta_1(t) = q_{\lambda 1}\zeta_1(t) \quad (4)$$

Elimination of $\zeta_1(t)$ is possible if two wavelengths λ_α and λ_β are selected:

$$\Delta A_{\lambda_\alpha}(t) = [q_{\lambda_\alpha 1}/q_{\lambda_\beta 1}]\Delta A_{\lambda_\beta}(t) \quad (5)$$

Thus, if an AD (absorbance difference) diagram, i.e., a plot of $\Delta A_{\lambda_\alpha}(t)$ vs $\Delta A_{\lambda_\beta}(t)$ at identical reaction times t is linear, then $s = 1$ (uniform reaction). A curved AD diagram indicates $s > 1$. This linearity holds for arbitrary wavelengths. However, for a good discrimination of linearity or nonlinearity of the plots, wavelengths in different parts of the spectrum, preferably in the spectral region of differing transitions, should be selected and several plots should be made.

In the case of $s = 1$ the A (absorbance) diagram according to

$$A_{\lambda_\alpha}(t) = aA_{\lambda_\beta}(t) + b \quad (6)$$

can be derived by similar arithmetics. The A diagram has the same diagnostic value as the AD diagrams.[34]

The Case $s = 2$. An example is

$$X \xrightarrow{\zeta_1(t)} B \xrightarrow{\zeta_2(t)} C$$

In a procedure analogous to that leading to eq 4, we can derive from the master equation (3)

$$\Delta A_\lambda(t) = q_{\lambda 1}\zeta_1(t) + q_{\lambda 2}\zeta(t) \quad (7)$$

The determination of the change of OD at three wavelengths λ_α, λ_β, and λ_β and subsequent elimination of $\zeta_1(t)$ and $\zeta_2(t)$ leads to

$$\Delta A_{\lambda_\alpha}(t) = a'\Delta A_{\lambda_\gamma}(t) + b'\Delta A_{\lambda_\beta}(t) \quad (8)$$

This is the equation of a plane in three-dimensional space. A projection parallel to this plane can be obtained to yield a straight line in a two-dimensional representation by rearrangement of eq 8 to give

$$\frac{\Delta A_{\lambda_\alpha}(t)}{\Delta A_{\lambda_\beta}(t)} = a'\frac{\Delta A_{\lambda_\gamma}(t)}{\Delta A_{\lambda_\beta}(t)} + b' \quad (9)$$

(31) Funke, U.; Grützmacher, A. F. *Tetrahedron* **1987**, *43*, 3787–3795.

(32) We thank Prof. Hohlneicher and Dr. Schönzart, Universität Köln, West Germany, for these experiments.

(33) Defined by $d\zeta = \nu_i\, dc_i$ in analogy to the common thermodynamic $d\xi = \nu_i\, dn_i$ (n = number of moles). In ref 27a, ζ is called X, in ref 27b, ζ is called λ.

(34) Mauser, H.; Niemann, H.-J.; Kretschmer, R. *Z. Naturforsch.* **1972**, *27B*, 1349–1352; Mauser, H.; Starrock, V.; Niemann, H.-J. *Z. Naturforsch.* **1972**, *27B*, 1354–1359.

Thus a nonlinear AD diagram and a linear ADQ2 (absorption difference quotient of second order) diagram indicate two independent reactions ($s = 2$). Nonlinear ADQ2 diagrams indicate higher order reactions ($s > 2$).[35]

The Case s > 2. Higher order diagrams have been developed[36] and interpreted in an analogous manner. They demand very high precision in measurement. If rate constants are very different from the others, lower order diagrams may be linear in restricted regions of the diagram.

(35) In some very special cases, e.g., if a linear ADQ2 plot happens to be parallel to an axis or goes through the origin, $s = 2$ and $s = 3$ cannot be discriminated by ADQ2 diagrams.

(36) Blume, R. Ph.D. Thesis, Tübingen, 1975.

(37) In cooperation with H. Mauser, Frauenstrasse, 7410 Reutlingen, West Germany.

Theoretical Studies of Nucleophilic Additions of Organocopper Reagents to Acrolein. Rationalization of the Differences in Regioselectivity in the Reactions of Methylcopper and Methyllithium

Andrea E. Dorigo and Keiji Morokuma*

Contribution from the Institute for Molecular Science, Myodaiji, Okazaki 444, Japan.
Received August 16, 1988

Abstract: Ab initio molecular orbital studies of the addition of methyllithium and methylcopper to acrolein have been performed. Transition states for addition to the carbonyl group (which gives the alcohol as the final product), to the carbon–carbon double bond, and across the π system (both of which lead to formation of the saturated ketone) have been located. Calculations at the HF/3-21G (with full geometry optimization), HF/6-31G*, and MP2/6-31G* levels indicate that reaction of methyllithium with the carbonyl group is preferred to conjugate addition to the double bond, in agreement with experimental data. In the computations of all species containing copper, an effective core potential was used in place of the inner-shell electrons, while the valence (3d, 4s, and 4p) orbitals were represented by basis sets of single- and double-ζ quality. Calculations at the HF/3-21G-ECP(SZ) and -ECP(DZ) levels were performed with full geometry optimization, and single-point energy calculations were carried out at the HF/6-31G*-ECP(DZ) and, in selected cases, MP2/6-31G*-ECP(DZ) and MP4/6-31G*-ECP(DZ) levels. All calculations indicate that 1,4-addition across the π system via a six-membered transition state is greatly favored over 1,2-addition. 1,4-Addition via a four-membered transition state is calculated to be slightly disfavored with respect to 1,2-addition to the carbonyl group. Possible reasons for the observed preference for 1,4-addition in solution are discussed.

The use of transition metal organometallic compounds in organic synthesis is a topic of established importance.[1] Among the several classes of systems which have found extensive application in the field, organocopper reagents deserve particular recognition. Ever since the early work by Kharasch and Tawney,[2] who pioneered the use of cuprous salts as catalysts in Grignard reactions, the number and scope of reagents containing copper has increased considerably.[3] The two most frequently used are the dialkylcuprates (generally with lithium as the counterion) and the alkylcopper–Lewis acid complexes. The latter species have been found to add regioselectivity (and often with high stereoselectivity) to the C=C bond of enones and enoates,[4] and to react with allylic substrates in S_N2' fashion almost exclusively.[5] The most common Lewis acids are boron trifluoride and aluminum trichloride, but several others have been employed effectively.[4] The precise mechanism of action is not known with certainty; however, Ganem has shown that the nucleophile and the Lewis acid act independently in the reaction of $LiCH_3$–BF_3 with oxiranes and oxetanes.[6] Here, the oxygen atom coordinates a molecule of boron trifluoride while the anionic methyl carbon attacks the C–O bond. This type of mechanism is likely to be valid whenever the electrophilic substrate contains strongly coordinating oxygen atoms.[4,7,8] Stereochemical studies of the addition of $MeCu{\cdot}AlCl_3$ to β'-cyclopropyl-α,β-enones show that the reaction mechanism does not involve electron transfer,[9] which has been postulated for the conjugate addition of lithium dialkylcuprates.[10]

This propensity for conjugate (1,4-) addition to α,β-unsaturated ketones (and esters) stands in sharp contrast to the preference

(1) *Transition Metal Organometallics in Organic Synthesis*; Alper, H., Ed.; Academic Press: New York, 1976; Vol. 1.

(2) Kharasch, M. S.; Tawney, P. O. *J. Am. Chem. Soc.* **1941**, *63*, 2308.

(3) Posner, G. H. *An Introduction to Synthesis Using Organocopper Reagents*; Wiley: New York, 1980. Collman, J. P.; Hegedus, L. S.; Norton, J. R.; Finke, R. G. *Principles and Applications of Organotransition Metal Chemistry*; University Science Books: Mill Valley, CA, 1987; Chapter 14.

(4) Yamamoto, Y. *Angew. Chem., Intl. Ed. Engl.* **1986**, *25*, 947.

(5) Goering, H. L.; Seitz, E. P., Jr.; Tseng, C. C. *J. Org. Chem.* **1981**, *46*, 5304. Goering, H. L.; Kantner, S. S.; Tseng, C. C. *J. Org. Chem.* **1983**, *48*, 715.

(6) Eis, M. J.; Wrobel, J. E.; Ganem, B. *J. Am. Chem. Soc.* **1984**, *106*, 3693.

(7) This seems true even for substrates other than α,β-unsaturated carbonyl compounds. Thus, acetals react with alkylcopper–Lewis acid reagents to give ethers: Ghribi, A.; Alexakis, A.; Normant, J. F. *Tetrahedron Lett.* **1984**, *25*, 3075.

(8) In contrast, Maruyama and Yamamoto have suggested that the reaction of $RCu{\cdot}BF_3$ with allylic halides involves the preliminary formation of an ate complex, $Cu^+BF_3(Me)^-$: Maruyama, K.; Yamamoto, Y. *J. Am. Chem. Soc.* **1977**, *99*, 8068.

(9) Ibuka, T.; Tabushi, E. *J. Chem. Soc., Chem. Commun.* **1982**, 703. Ibuka, T.; Tabushi, E.; Yasuda, M. *Chem. Pharm. Bull.* **1983**, *31*, 128.

(10) House, H. O. *Acc. Chem. Res.* **1976**, *9*, 59. House, H. O.; Chu, C-Y. *J. Org. Chem.* **1976**, *41*, 3083. Yamamoto, Y.; Shinji, N.; Ibuka, T. *J. Am. Chem. Soc.* **1988**, *110*, 617. Evidence *against* this type of mechanism has been found by Bertz and Cook: Bertz, S. H.; Dabbagh, G.; Cook, J. M.; Honkan, V. *J. Org. Chem.* **1984**, *49*, 1739; and by Jullien: Frejaville, C.; Jullien, R.; Stahl-Lariviere, H.; Wanat, M.; Zann, D. *Tetrahedron* **1982**, *38*, 2671.

0002-7863/89/1511-4635$01.50/0